BJ www.biochemj.org

BJ Signal

Biochem. J. (2010) **430**, 439–451 (Printed in Great Britain) doi:10.1042/BJ20100503

439

online data

p38^{MAPK}/p53 signalling axis mediates neuronal apoptosis in response to tetrahydrobiopterin-induced oxidative stress and glucose uptake inhibition: implication for neurodegeneration

Simone CARDACI*[1], Giuseppe FILOMENI*[1], Giuseppe ROTILIO*† and Maria R. CIRIOLO*†[2]

*Department of Biology, University of Rome "Tor Vergata", Via della Ricerca Scientifica 1, 00133 Rome, Italy, and †Research Centre IRCCS San Raffaele - Pisana, Via dei Bonacolsi, 00163 Rome, Italy

BH4 (tetrahydrobiopterin) induces neuronal demise via production of ROS (reactive oxygen species). In the present study we investigated the mechanisms of its toxicity and the redox signalling events responsible for the apoptotic commitment in SH-SY5Y neuroblastoma cells and in mouse primary cortical neurons. We identified in p38^{MAPK}/p53 a BH4-responsive pro-apoptotic signalling axis, as demonstrated by the recovery of neuronal viability achieved by gene silencing or pharmacological inhibition of both p38^{MAPK} and p53. BH4-induced oxidative stress was characterized by a decrease in the GSH/GSSG ratio, an increase in protein carbonylation and DNA damage. BH4 toxicity and the redox-activated apoptotic pathway were counteracted by the H_2O_2-scavengers catalase and *N*-acetylcysteine and enhanced by the GSH neo-synthesis inhibitor BSO (buthionine sulfoximine). We also demonstrated that BH4 impairs glucose uptake and utilization, which was prevented by catalase administration. This effect contributes to the neuronal demise, exacerbating BH4-induced nuclear damage and the activation of the pro-apoptotic p38^{MAPK}/p53 axis. Inhibition of glucose uptake was also observed upon treatment with 6-hydroxydopamine, another redox-cycling molecule, suggesting a common mechanism of action for auto-oxidizable neurotoxins.

Key words: apoptosis, glucose, glutathione, mitogen-activated protein kinase (MAPK), p53, reactive oxygen species (ROS).

INTRODUCTION

Oxidative stress is considered to be an important pathogenetic factor in several neurodegenerative diseases such as PD (Parkinson's disease) and AD (Alzheimer's disease). Because of its high metabolic rate and relatively reduced capacity for cellular regeneration compared with other organs, the brain is believed to be particularly susceptible to the damaging effects of ROS (reactive oxygen species). This vulnerability is highlighted by the accumulation of protein carbonyls and lipid hydroperoxides, as well as a decrease in glutathione (GSH) levels both in experimental models of neurological disorders and in *post-mortem* PD and AD brains [1–3]. One of the main determinants of oxidative-dependent neuronal degeneration is the impairment of neuronal bioenergetics. Although mitochondria are the best defined ATP-producing structures that are affected oxidatively in several neurological disorders, a growing number of reports indicate that ROS play a pivotal role in the hypometabolism of glucose as well. Positron emission tomography analyses demonstrate that glucose utilization is reduced in several regions of AD and PD brains [4,5]. Moreover, the decline in glucose metabolism appears before the onset of cognitive deficits and seems to sensitize neurons to further energy deficiency and oxidative damage [6–8].

The involvement of oxidative stress in neuronal demise is strengthened by the activation of pro-apoptotic transcription factors, such as p53 [9]. Particularly, the insensitivity of p53-null mice to the dopaminergic neurotoxin MPTP (1-methyl-4-phenyl-1,2,3,6-tetrahydropyridine), as well as the resistance observed in mice treated with the p53 inhibitor pifithrin-α, demonstrate the involvement of p53 in PD pathogenesis [10,11]. Moreover, a pivotal role in the degeneration of neurons seems to be played by the MAPKs (mitogen-activated protein kinases). Indeed, the accumulation of phospho-active JNK (c-Jun N-terminal kinase) and p38^{MAPK} have been detected in post-mortem PD and AD brains, and their pharmacological inhibition induces neuroprotection [12–14].

The enhanced vulnerability of neurons to pro-oxidant settings is exacerbated by the high concentration of redox-active metals in several brain regions and the presence of neuron-specific molecules such as dopamine and neuromelanine, whose metabolism generates ROS. Among the redox-cycling molecules fundamental for brain metabolism, BH4 (tetrahydrobiopterin) plays a pivotal role both in neurons and glial cells acting as a cofactor for aromatic *L*-amino acid hydroxylases and NOS (NO synthase) in catecholamines and nitric oxide synthesis respectively. Despite its important physiological functions, recent studies demonstrate the implication of BH4 in neuronal apoptosis.

Abbreviations used: AD, Alzheimer's disease; AMPK, AMP-activated protein kinase; ARE, AU-rich region; BH4, tetrahydrobiopterin; BSO, buthionine sulfoximine; DAF-DA, 4,5-diaminofluorescein diacetate; DCFH-DA, 2′,7′-dichlorodihydrofluorescein diacetate; DMEM, Dulbecco's modified Eagle's medium; DNP, 2,4-dinitrophenylhydrazine; FCS, fetal calf serum; GAPDH, glyceraldehyde-3-phosphate dehydrogenase; GLUT, glucose/hexose transporter; HBSS, Hepes-buffered salt solution; JNK, c-Jun N-terminal kinase; L-NAME, N^G-nitro-L-arginine methyl ester; MAPK, mitogen-activated protein kinase; MKK3/6, MAPK kinase 3/6; MPTP, 1-methyl-4-phenyl-1,2,3,6-tetrahydropyridine; NAC, *N*-acetylcysteine; 2-NBDG, 2-[*N*-(7-nitrobenz-2-oxa-1,3-diazol-4-yl) amino]-2-deoxy-D-glucose; 7-Ni, 7-nitroindazole; NOS, NO synthase; 6-OHDA, 6-hydroxydopamine; PARP, poly(ADP-ribose) polymerase; PCN, primary cortical neuron; PD, Parkinson's disease; ROS, reactive oxygen species; siRNA, small interfering RNA; Z-VAD-FMK, benzyloxycarbonyl-Val-Ala-DL-Asp-fluoromethylketone.

[1] These authors contributed equally to this work.

[2] To whom correspondence should be addressed (email ciriolo@bio.uniroma2.it).

Indeed, the exposure of neuronal cell lines and primary cultured rat neurons to BH4 [15,16] results in the occurrence of oxidative damage and neuronal cell death, consistent with the current view of parkinsonism. In particular, it has been reported that intrastriatal and intraventricular injections of BH4 induce the preferential loss of dopaminergic cells of the nigro-striatal pathway, combined with a motor deficit related to dopamine depletion [17,18]. Although intracellular BH4 concentration (estimated to be 100 μM) [19] is not toxic, probably due to the high neuronal reducing environment, extracellular BH4 is detrimental for neuron viability. Moreover, BH4 can be over-produced in catecholaminergic cells in response to calcium increase or stress conditions and released from neurons and activated glia [20–22]. Therefore neurons can be exposed to relatively high levels of BH4 in the brain, giving it physiological relevance in neurodegenerative settings. Although the toxic effects of BH4 seem to be dependent on ROS generated during its auto-oxidation, as well as during the enzymatic catalysis of tyrosine hydroxylase [23], the molecular mechanisms underlying its toxicity have not been completely characterized yet.

In the present study we investigated the signalling pathways activated in response to BH4 challenge in neuronal cells. We demonstrated that BH4 induces inhibition of glucose uptake as a consequence of its ability to produce ROS. The reduced glucose availability and utilization contribute to the neuronal demise, exacerbating BH4-induced oxidative stress and the commitment of SH-SY5Y cells and mouse primary cortical neurons to apoptosis via activation of the $p38^{MAPK}$/p53 axis.

MATERIALS AND METHODS

Materials

BH4 and Z-VAD-FMK (benzyloxycarbonyl-Val-Ala-DL-Asp-fluoromethylketone) were from Alexis. BSO (buthionine sulfoximine), catalase, pifithrin-α, EDTA, EGTA, NAC (*N*-acetyl-cysteine), paraformaldehyde, propidium iodide, Triton X-100, L-NAME [N^G-nitro-L-arginine methyl ester], 7-Ni (7-nitroindazole) and 6-OHDA (6-hydroxydopamine) were from Sigma. Goat anti-mouse and anti-rabbit IgG (heavy and light chains)–horseradish peroxidase conjugate were from Bio-Rad Laboratories. Neurobasal medium, B27 supplement, 2-NBDG {2-[*N*-(7-nitrobenz-2-oxa-1,3-diazol-4-yl) amino]-2-deoxy-D-glucose}, DCFH-DA (2′,7′-dichlorodihydrofluorescein diacetate) and DAF-DA (4,5-diaminofluorescein diacetate) were from Invitrogen-Molecular Probes. JNK inhibitors I and II, the $p38^{MAPK}$ inhibitor SB203580 and Hoechst 33342 were from Calbiochem. All other chemicals were obtained from Merck.

SH-SY5Y cell culture

Human neuroblastoma SH-SY5Y cells were purchased from the European Collection of Cell Culture and grown in DMEM (Dulbecco's modified Eagle's medium)-F12 supplemented with 10 % FCS (fetal calf serum), 1 % penicillin/streptomycin and 1 % glutamine. The cells were maintained at 37 °C in a 5 % CO_2 atmosphere in air and routinely trypsinized and plated at 4×10^4/cm^2 on flasks. Cell viability was assessed by Trypan Blue exclusion.

Glucose-free culture conditions were achieved using the method of Bellucci et al. [7]. Briefly, the SH-SY5Y cell line was incubated in 15 mM HBSS (Hepes-buffered salt solution), pH 7.45, supplemented with 10 % FCS, 0.01 mM non-essential amino acids, 1 % penicillin/streptomycin and 1 % glutamine without glucose. As control, cells were grown in the same medium supplemented with 16 mM glucose, which corresponds to the concentration present in DMEM/F12 medium.

Mouse primary cortical neurons

Mouse PCNs (primary cortical neurons) were obtained from cerebral cortices of E15 (embryonic day 15) C57BL-6 mice embryos. All the experiments were performed according to the Animal Research Guidelines of the European Communities Council Directive (86/609/EEC). Minced cortices were digested with 0.25 % trypsin (Lonza)/EDTA at 37 °C for 7 min. Cells were stained with 0.08 % Trypan Blue solution and only viable cells were counted and plated at a density of 10^5/cm^2 on to poly-D-lysine-coated coverlips or multiwell plates in 25 mM glucose-containing MEM (minimal essential medium) supplemented with 10 % FCS, 2 mM glutamine and 0.1 mg/ml gentamicin (Invitrogen). After 1 h, the medium was replaced with Neurobasal medium containing antioxidant-free B27 supplement (Invitrogen), 2 mM glutamine and 0.1 mg/ml gentamicin. Cell cultures were kept at 37 °C in a humidified atmosphere containing 5 % CO_2. Every 3 days, one third of the medium was replaced up to day 7, at the time at which the cells were treated. Glucose-free culture conditions were performed by culturing PCNs in HBSS supplemented with B27, 0.01 mM non-essential amminoacids, 1 % gentamicin and 1 % glutamine without glucose. As control, PCNs were grown in the same medium supplemented with 25 mM glucose, which correspond to the concentration present in neurobasal medium.

Transfections

At 24 h after plating, 50 % confluent SH-SY5Y cells were transfected with two alternative siRNA (small interfering RNA) duplexes directed against the p53 mRNA target sequence provided respectively by MWG Biotech (Ebersberg, Germany) (sip53) and Thermo Fisher Scientific (Dharmacon, Lafayette, CO, U.S.A) (sip53-2). Similarly, $p38^{MAPK}$ knockdown was achieved by tranfecting the cells with a SignalSilence® Pool $p38^{MAPK}$ siRNA (Cell Signaling Technology) ($sip38^{MAPK}$) or with an ON-TARGET*plus* $p38^{MAPK}$ siRNA (Thermo Fisher Scientific) (sip38-2). Control cells were transfected with two different scramble siRNA duplexes (siScr and siScr-2), which do not present homology with any other human mRNAs. Plasmid transfections were performed with a pcDNA3 empty vector or with a pcDNA3 vector containing the FLAG-tagged coding sequence for the α1 subunit of $p38^{MAPK}$ carrying the replacement of Thr^{180} and Tyr^{182} with two non-phosphorylatable residues, alanine and phenylalanine respectively (provided by Professor Jiahuai Han, The Scripps Research Institute, Department of Immunology, North Torrey Pines Road, La Jolla, CA, U.S.A.). Cell transfection was performed as previously described [25].

Treatments

A 10 mM solution of BH4 was prepared just before the experiments by dissolving the powder in water. Treatments were performed at final concentrations ranging from 0.5 to 200 μM, in medium. As control, equal volumes of water were added to untreated cells. The concentration of 100 μM and 1 μM BH4 were selected for the following experiments in SH-SY5Y cells and PCNs respectively, if not otherwise indicated, because they allowed the evaluation of a reliable apoptotic degree in a time-window of 24 h. The pan-caspase inhibitor Z-VAD-FMK and the p53 inhibitor pifithrin-α were used at 20 μM, pre-incubated for 1 h before the addition of BH4, and maintained throughout the experiment. BSO was used at a final concentration of 1 mM or

25 μM in SH-SY5Y cells and PCNs respectively, added 12 h before BH4 addition and maintained throughout the experiment. JNK inhibitors I and II were used at a concentration of 10 μM. The p38^{MAPK} inhibitor SB203580 was used at a concentration of 15 μM. NAC was used at a final concentration of 5 mM. After 12 h of incubation, the cells were rinsed with PBS and transferred to fresh NAC-free medium. Catalase (1 μM) was added 1 h before BH4 addition and maintained in the medium throughout the experimental time. NOS inhibitors L-NAME and 7-Ni were used at concentrations of 100 μM and 10 μM respectively, pre-incubated for 1 h before BH4 addition and maintained throughout the experiment.

Analysis of cell viability and apoptosis

Adherent (after trypsinization) and detached SH-SY5Y cells were combined, washed with PBS and stained with 50 μg/ml propidium iodide prior to analysis by a FACScalibur instrument (Becton Dickinson). The percentages of apoptotic cells were evaluated using the method of Nicoletti et al. [26]. Determination of PCN apoptosis was performed evaluating nuclear morphology by fluorescence microscopy after incubation with the cell-permeant dye Hoechst 33342. The percentages of apoptotic cells were evaluated by counting nuclei displaying condensed or fragmented chromatin in six subfields of each culture. All experiments were performed at least three times with similar results.

Measurement of NO levels

Intracellular NO production was determined by flow cytometry using the cell-permeant NO-specific probe DAF-DA according to the manufacturer's instructions.

Western blot analyses

Total protein extracts were obtained as previously described [27]. Protein extracts were then separated by SDS/PAGE (10–12% gels) and blotted on to a nitrocellulose membrane (Bio-Rad Laboratories). Monoclonal anti-p53 (clone BP5312), anti-actin (Sigma); anti-phospho-Thr^{172} of AMPK (AMP-activated protein kinase) α-subunits, anti-caspase-3 (clone 3G2 - Cell Signaling Technology); anti-GAPDH (glyceraldehyde-3-phosphate dehydrogenase), anti-phospho-JNK1, anti-phospho-c-Jun, anti-PARP [poly(ADP-ribose) polymerase] (Santa Cruz Biotechnology); polyclonal anti-AMPK, anti-Bax, anti-JNK, anti-p38^{MAPK} (Santa Cruz Biotechnology); anti-caspase-9 (Cell Signaling Technology); and anti-phospho-Thr^{180}/Tyr^{182} p38^{MAPK} (Invitrogen) were used as primary antibodies. The specific protein complex, formed upon specific secondary antibody treatment, was identified using a Fluorchem Imaging system (Alpha Innotech, M-Medical, Milano, Italy) after incubation with ChemiGlow chemiluminescence substrate (Alpha Innotech).

Measurement of oxidative stress

Intracellular GSH and GSSG and external plasma membrane thiols were analysed as previously described [27]. Detection of intracellular ROS by DCFH-DA was performed as previously described [28]. Carbonylated proteins were detected using the Oxyblot Kit (Intergen) after reaction with DNP (2,4-dinitrophenylhydrazine) for 15 min at 25 °C. Samples were then resolved by SDS/PAGE (10 % gels) and DNP-derivatized proteins were identified by immunoblotting using an anti-DNP antibody [29].

Fluorescence microscopy analyses

Cells were plated on chamber slides at 6×10^4/cm^2, fixed with 4 % paraformaldehyde and permeabilized. For the determination of DNA damage, they were washed with PBS, blocked with PBS containing 10 % FCS, incubated with a monoclonal anti-(Ser^{139}-phosphorylated histone H2A.X) antibody (clone JBW301; Upstate Biotechnology), and further probed with Alexa Fluor®-488-conjugated secondary antibody (Molecular Probes). For the determination of p38^{MAPK} and p53 activation/localization, cells were stained with a polyclonal anti-phospho-Thr^{180}/Tyr^{182}-p38^{MAPK} antibody and with a monoclonal (Sigma) or polyclonal anti-p53 (Santa Cruz Biotechnology) for SH-SY5Y cells or PCNs respectively. Slides were further probed with Alexa Fluor®-488 and Alexa Fluor®-568-conjugated secondary antibodies to visualize phospho-p38^{MAPK} and p53 respectively. To highlight nuclei, cells were also incubated with the cell-permeant DNA dye Hoechst 33342 (Calbiochem–Novabiochem). Images of cells were acquired and digitized with a Delta Vision Restoration Microscopy System (Applied Precision) equipped with an Olympus IX70 fluorescence microscope.

Extracellular lactate assay

Extracellular lactate concentration was assessed as previously described [30].

Measurement of glucose uptake

SH-Y5Y cells and PCNs were incubated for the indicated experimental time with 100 μM 2-NBDG, a fluorescent derivative of 2-deoxy-D-glucose, in the presence or absence of 1 μM catalase. Cells were exhaustively washed with PBS to stop 2-NBDG uptake and collected, and fluorescence was analysed cytofluorimetrically.

Data collection

Protein concentrations were determined by the method of Lowry et al. [31]. All experiments were performed at least three separate times unless otherwise indicated. Data are expressed as means $\pm$ S.D. and significance was assessed by Student's t test corrected by Bonferroni's method. Differences with P values <0.05 were considered significant.

RESULTS

BH4 elicits a caspase-dependent apoptosis in neuronal cells

The cytotoxic effects of BH4 were determined in the neuroblastoma cell line SH-SY5Y. Figure 1(A) shows cytofluorimetric analyses of SH-SY5Y cells treated for 24 h with different concentrations of BH4 (50–200 μM). Consistent with data presented previously in the literature [32,33], a dose-dependent increase in the percentage of apoptotic cells (sub-G_1 region of the histogram) was shown. Then, to characterize the apoptotic process, we analysed caspase activation by Western blotting. Figure 1(B) shows that BH4 treatment induced the cleavage of caspase-9 and caspase-3, as well as the proteolysis of PARP, starting from 6 h of treatment. Moreover, the recovery of cell viability (see Supplementary Figure S1 at http://www.BiochemJ.org/bj/430/bj4300439add.htm), achieved by treating the cells with the pan-caspase inhibitor Z-VAD-FMK, demonstrated that the caspase-mediated apoptosis was the principal mechanism of cell death. In order to corroborate the results of SH-SY5Y cells, we moved on to mouse PCNs, widely employed to investigate the pro-apoptotic mechanisms of neurotoxic molecules. We treated PCNs for 24 h with various concentrations of BH4 (1–50 μM)

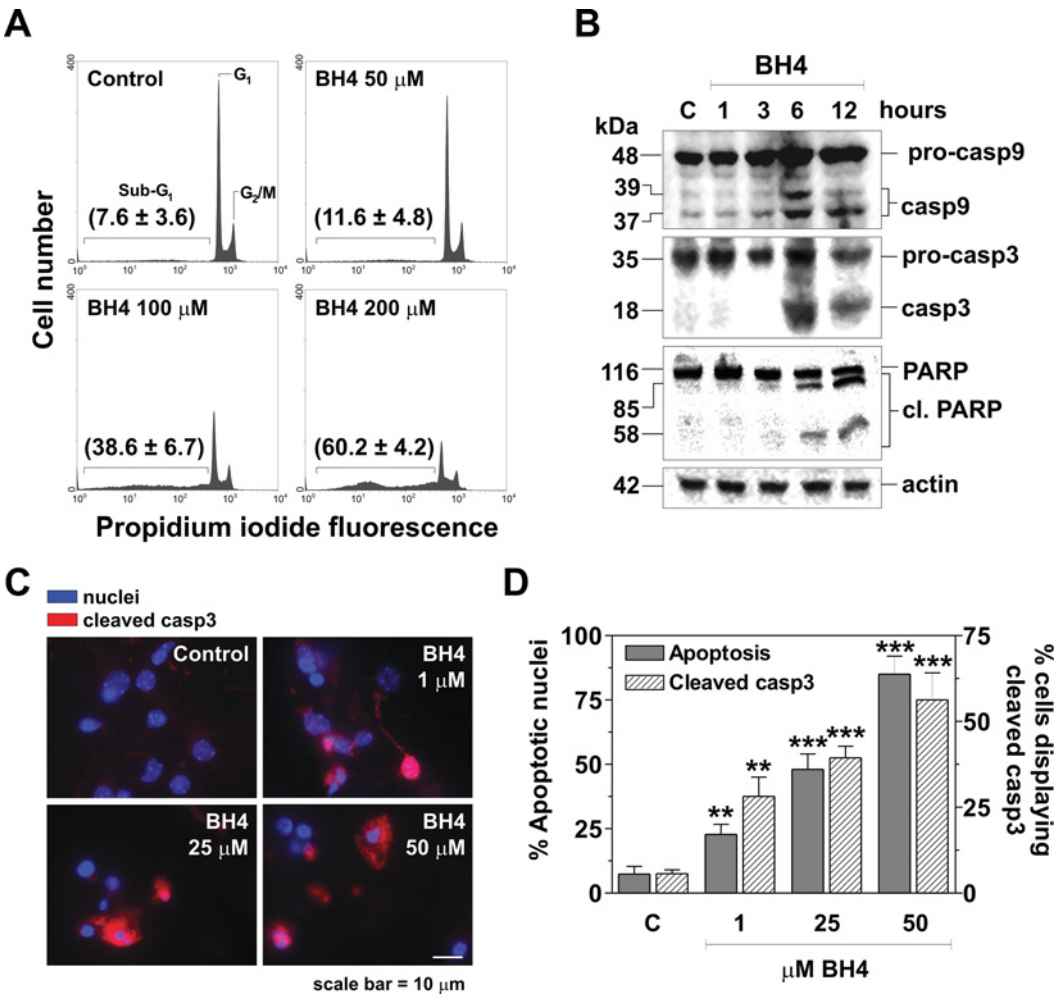

Figure 1 BH4 induces apoptosis in neuronal cells

(**A**) SH-SY5Y cells were treated with 50–200 μM BH4 for 24 h, then washed and stained with propidium iodide. Analysis of cell cycle and apoptosis were performed using a FACScalibur instrument and percentages of positive-staining cells were calculated using WinMDI version 2.8 software. Cell cycle plots reported are from a typical experiment performed in triplicate out of five that gave similar results. (**B**) SH-SY5Y cells were treated with 100 μM BH4. At the indicated times, cells were lysed and 30 μg of total cell extracts were loaded for the immunodetection of caspase-9, caspase-3 and PARP. Actin was used as a loading control. Immunoblots are from one experiment representative of three that gave similar results. casp, caspase; cl. PARP, cleaved PARP. Molecular masses are given in kDa to the left. (**C** and **D**) PCNs were treated with 1–50 μM BH4 for 24 h, washed, fixed in 4 % paraformaldehyde and permeabilized. Cleaved caspase-3 was visualized upon staining with a specific antibody and further probed with Alexa Fluor® -568-conjugated secondary antibody. To visualize nuclei, cells were also incubated with the cell-permeant DNA dye Hoechst 33342. Representative images (**C**) and the percentages of cells with apoptotic nuclei and cleaved caspase-3 (**D**) are shown. Values are means ± S.D. ($n = 5$). $^{**}P < 0.01$; $^{***}P < 0.001$.

and analysed apoptosis engagement by counting condensed and fragmented nuclei upon Hoechst staining and by evaluating caspase-3 cleavage by fluorescence microscopy. Also in this case, BH4 exhibited a marked neurotoxicity. Indeed, cleaved-caspase-3 and apoptotic nuclei were detectable upon 24 h of treatment with 1 μM BH4 (Figures 1C and 1D). On the basis of these results, the concentrations of 100 μM and 1 μM BH4 were selected for the following experiments in SH-SY5Y cells and PCNs respectively.

BH4-induced neuronal apoptosis is a ROS-mediated event

BH4 is a cofactor of neuronal NOS, therefore it has a prominent role in NO generation. To assess whether nitrosative stress underlays BH4 toxicity, we treated SH-SY5Y cells with BH4 and cytofluorimetrically measured both NO levels and apoptosis upon NOS inhibition with 10 μM 7-Ni or 100 μM L-NAME. Neither an increase in NO production nor modulation of cell viability was detectable (results not shown), indicating that NO was not involved in BH4 neurotoxicity. Next, we focused on the capability of BH4 to induce oxidative stress. We measured ROS content cytofluorimetrically by incubating SH-SY5Y cells with 5 μM of DHDCF-DA. Figure 2(A) shows that ROS accumulated intracellularly starting from 30 min of treatment. The rapid kinetics of ROS production prompted us to analyse the content of the tripeptide glutathione. HPLC analyses revealed that both the reduced (GSH) and the oxidized (GSSG) form of glutathione were affected by BH4 treatment in neuroblastoma cells. In particular, as depicted in Figure 2(B), GSH significantly decreased already at 30 min after BH4 administration, whereas GSSG increased during the treatment, suggesting a buffer role for GSH against ROS-mediated oxidative stress. On the basis of these results, we wondered whether the integrity of proteins and DNA, two well-known targets of ROS-mediated damage, was also affected. DNA damage was evaluated by fluorescence microscopy analyses of the phospho-activation of the DNA double-strand-break-sensitive histone H2A.X. Figure 2(C) shows that BH4 treatment caused a time-dependent appearance

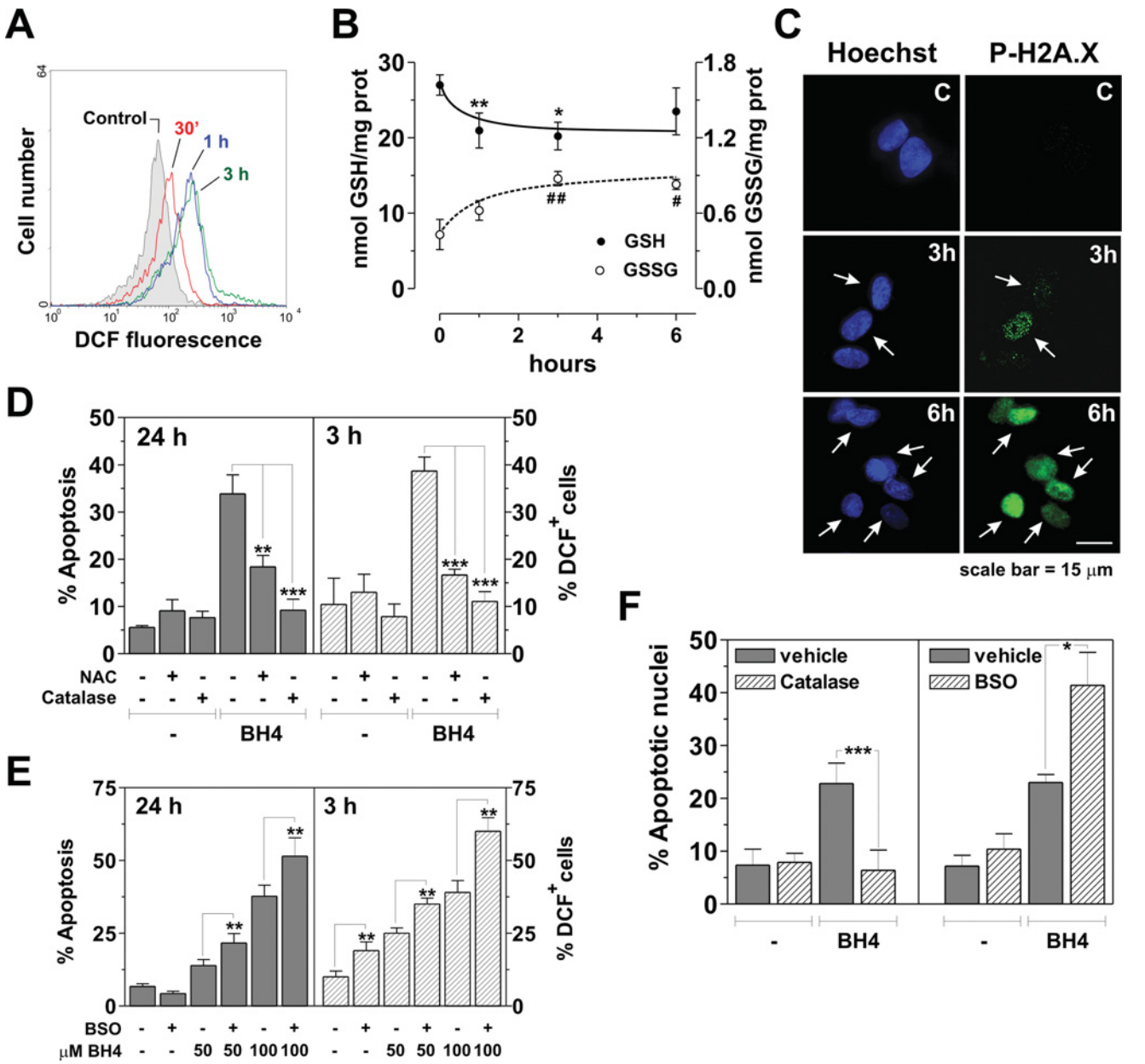

Figure 2 BH4 elicits oxidative stress in neuronal cells

(**A**) SH-SY5Y cells were treated with 100 μM BH4 for 30 min, 1 or 3 h, and incubated with 50 μM DCF-DA at 37 °C. At the indicated time points, cells were washed with PBS and ROS production was analysed using a FACScalibur instrument. Histograms shown are representative of three experiments that gave similar results. (**B**) SH-SY5Y cells were treated with 100 μM BH4. At the indicated times, cells were collected, exhaustively washed with PBS and assayed for GSH and GSSG using HPLC. Data are expressed as nmol of GSH or GSSG/mg of total proteins and are means $\pm$ S.D. ($n = 5$). For GSH: $^{*}P < 0.05$; $^{**}P < 0.01$. For GSSG: $^{\#}P < 0.05$; $^{\#\#}P < 0.01$. (**C**) SH-SY5Y cells were treated with 100 μM BH4. At the indicated times, cells were fixed with paraformaldehyde and subjected to immunostaining with an anti-phospho-H2A.X antibody (P-H2A.X) and which was detected with Alexa Fluor®-488-conjugated secondary antibody. Nuclei were stained with Hoechst 33342. Images reported are from one experiment of three that gave similar results. SH-SY5Y cells were treated with 100 μM BH4 upon 12 h of incubation with 5 mM NAC or in the presence of 1 μM catalase (**D**), or with 1 mM BSO (**E**). After 3 h, cells were incubated for further 30 min with 50 μM DCF-DA at 37 °C, washed with PBS and ROS production was analysed using a FACScalibur instrument. Data are expressed as %DCF^{+} (% of DCF-positive) cells. After 24 h, cells were stained with propidium iodide. Analysis of sub-G_1 (apoptotic) cells was performed using a FACScalibur instrument. Data are expressed as percentages of apoptosis. Values are the means $\pm$ S.D ($n = 5$). $^{**}P < 0.01$; $^{***}P < 0.001$. (**F**) PCNs were treated with 1 μM BH4 in the presence of 1 μM catalase, or with 1 mM BSO. After 24 h, cells were stained with Hoechst 33342 and condensed or fragmented nuclei were counted as apoptotic. Data are expressed as percentages of apoptotic nuclei. Values are the means $\pm$ S.D. ($n = 5$). $^{*}P < 0.05$; $^{***}P < 0.001$.

of discrete nuclear foci, indicating the recruiting sites of the DNA repair systems, thus revealing the occurrence of DNA-specific damage. Protein oxidation was assessed by evaluating carbonyl content and protein thiols located at the exofacial side of the plasma membrane. Supplementary Figure S2(A) (at http://www.BiochemJ.org/bj/430/bj4300439add.htm) shows that proteins were efficiently carbonylated in a time-dependent manner. Also, a marked decrease in reduced thiols occurred upon staining with the impermeant thiol-reacting compound Alexa Fluor® 488–C_5-maleimide (Supplementary Figure S2B), confirming the oxidative challenge.

To verify the direct association between BH4-induced oxidative stress and the occurrence of apoptosis, we pre-incubated the cells for 12 h with 5 mM NAC to increase the intracellular thiol pool,

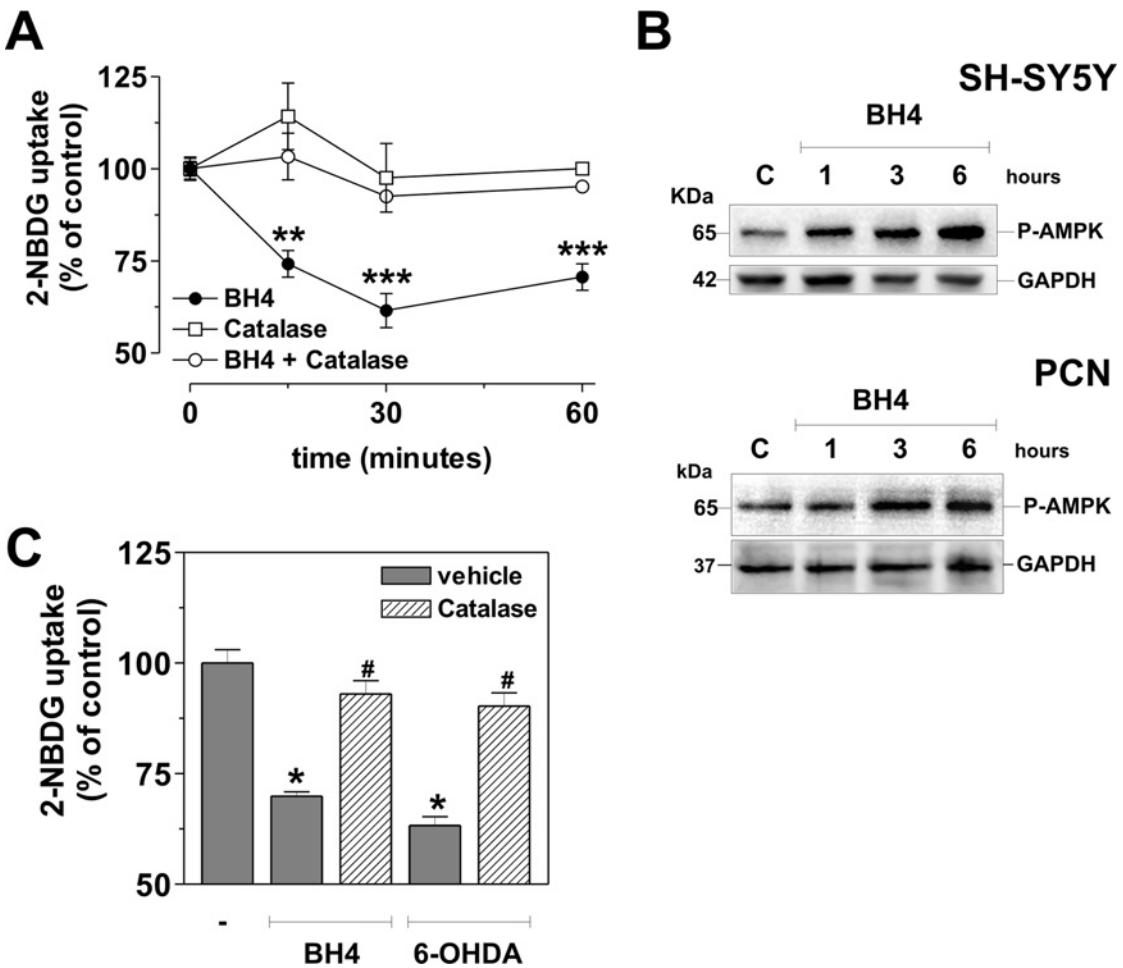

Figure 3 BH4 induces glucose uptake inhibition

(**A**) SH-SY5Y cells were treated with 100 μM BH4 for 1 h in the presence or absence of 1 μM catalase and replaced with fresh medium containing 100 μM 2-NBDG. After 15, 30 or 60 min, cells were washed to stop 2-NBDG uptake, collected and cytofluorimetrically analysed. Data are expressed as percentages of decrease with respect to untreated (control) cells and are means $\pm$ S.D., $n = 6$. $^{**}P < 0.01$; $^{***}P < 0.001$. (**B**) SH-SY5Y cells and PCNs were treated with 100 μM and 1 μM BH4 respectively. At the indicated times, cells were lysed and 30 μg of total cell extracts were loaded for the immuno-detection of the phosphorylated activated form of AMPK (P-AMPK). GAPDH was used as loading control. Immunoblots are from one experiment representative of three that gave similar results. (**C**) PCNs were treated with 1 μM BH4, or, alternatively, 5 μM 6-OHDA in the presence or absence of 1 μM catalase. After 30 min, 2-NBDG fluorescence was analysed cytofluorimetrically. Data are expressed as percentages of decrease with respect to untreated (control) cells and represent the means $\pm$ S.D., $n = 6$. BH4 or 6-OHDA treated cells compared with control, $^{*}P < 0.05$; compared with catalase co-administration, $^{\#}P < 0.05$.

or with 1 μM catalase, an H_2O_2 dismutating enzyme. We then measured ROS content after 3 h of incubation with BH4 as well as apoptotic extent after 24 h of treatment. Figure 2(D) shows that both of the antioxidants prevented ROS production and cell death, even though catalase seemed to be more efficient. Since the GSH/GSSG ratio also appeared to be profoundly affected upon BH4 treatment, we induced GSH depletion by 12 h of pre-treatment with 1 mM BSO, an irreversible inhibitor of GSH neo-synthesis. Figure 2(E) shows that GSH depletion resulted in increased ROS levels and an enhanced vulnerability towards BH4. The involvement of oxidative stress in the induction of apoptosis was also confirmed to be operative in neurons, as demonstrated by the complete recovery of PCN viability achieved by catalase addition to cell medium (Figure 2F) as well as the enhanced sensitivity to BH4 obtained by incubating PCNs with 25 μM BSO (Figure 2F). These results, in line with previous investigations performed with other PD neurotoxins [34], confirm that oxidative stress is the principal event leading to BH4-induced neuronal apoptosis.

BH4 induces glycolytic impairment in neuronal cells

Some pieces of evidence from the literature suggest a relationship among cellular redox state, glucose metabolism and neurodegeneration [8,35]. Therefore we wondered whether ROS produced downstream of BH4 auto-oxidation could affect cellular energetics. To this aim, we focused on the possible impairment of glucose uptake by evaluating the incorporation of 2-NBDG, the fluorescent analogue of 2-deoxy-D-glucose. Figure 3(A) shows that cells treated for 1 h with 100 μM BH4 exhibited a decrease in 2-NBDG uptake (approx. -40 % with respect to untreated cells). Moreover, if the cells were pre-incubated with 1 μM catalase, no change in 2-NBDG fluorescence was observed, indicating that catalase was able to completely restore glucose uptake at rates similar to those of control (Figure 3A). We then performed a lactate assay in culture media. Supplementary Figure S3 (at http://www.BiochemJ.org/bj/430/bj4300439add.htm) shows that extracellular lactate, which represents a measure of glycolytic metabolism, significantly decreased after 6 h of treatment with

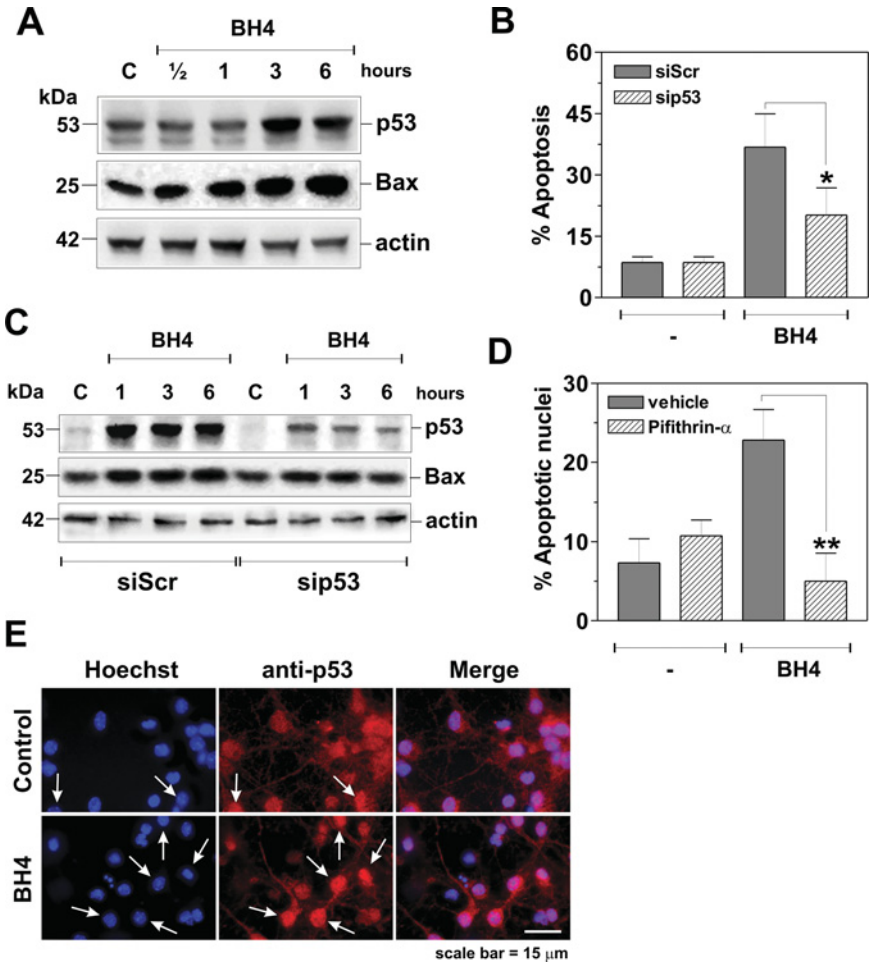

Figure 4 p53 activation is functional for BH4-induced apoptosis

(**A**) SH-SY5Y were treated with 100 μM BH4. At the indicated times, cells were lysed and 30 μg of total cell extracts were loaded for the immunodetection of p53 and Bax. Actin was used as a loading control. Immunoblots are from one experiment representative of three that gave similar results. (**B**) SH-SY5Y cells were transiently transfected with siRNA duplex directed against the p53 mRNA target sequence (sip53) or with a scramble siRNA duplex (siScr), which does not present homology with any other human mRNAs. Cell adhesion was allowed for 12 h, then the cells were treated with 100 μM BH4 for the next 24 h, washed and finally stained with propidium iodide for the detection of apoptotic cells. Data are expressed as percentages of apoptosis and are means $\pm$ S.D., $n = 6$. $^{*}P < 0.05$. (**C**) After 12 h of transfection with siScr or sip53, SH-SY5Y cells were treated with 100 μM BH4. At the indicated times, cells were lysed and 30 μg of total cell extracts were loaded for the immunodetection of p53 and Bax. Actin was used as a loading control. Immunoblots are from one experiment representative of three that gave similar results. (**D**) PCNs were treated with 1 μM BH4 for 24 h,washed, fixed in 4 % paraformaldehyde and permeabilized. p53 was visualized upon staining with specific antibody which was detected with Alexa Fluor®-568-conjugated secondary antibody. Nuclei were visualized by incubation with Hoechst 33342. Images reported are from one experiment representative of three that gave similar results. White arrows indicate representative cells where anti-p53 and Hoechst fluorescences superimpose. (**E**) PCNs were treated with 1 μM BH4 in the presence or absence of 20 μM pifithrin-α. After 24 h, cells were stained with Hoechst 33342 and condensed or fragmented nuclei were counted as apoptotic. Data are expressed as percentages of apoptotic nuclei. Values are means $\pm$ S.D, $n = 5$. $^{**}P < 0.01$.

BH4, a phenomenon that was completely prevented by pre-incubation with catalase. To confirm a bioenergetic unbalance following glucose uptake inhibition, we monitored phospho-activation of AMPK, an energetic-stress-responsive kinase activated downstream of an AMP/ATP ratio increase [36]. Despite the basal amount of protein not changing during BH4 treatment (results not shown), Western blot analyses of phosphorylated/activated AMPK (P-AMPK) indicates that it accumulated time-dependently as early as 1 h (Figure 3B). Similarly, PCNs treated with 1 μM BH4 showed a significant decrease in glucose uptake that was recovered by the addition of catalase (Figure 3C), as well as a time-dependent activation of AMPK (Figure 3B). To investigate further whether the ability to impair glucose accumulation was a feature shared with other neurotoxins generating extracellular ROS, we measured 2-NBDG uptake in PCNs after 1 h of challenge with 5 μM 6-OHDA, another redox-cycling molecule. Figure 3(C) shows that, similarly to BH4, 6-OHDA was also able to reduce 2-NBDG accumulation in a ROS-dependent manner. Indeed, the addition of catalase completely restored 2-NBDG uptake, suggesting that alterations in glucose homoeostasis could contribute to neuronal demise induced by redox-active PD toxins.

p53 is involved in BH4-induced neuronal apoptosis

To dissect the signalling pathway(s) involved in BH4-induced apoptosis, we focused on p53, whose induction has been correlated with neuronal degeneration. We treated SH-SY5Y cells with 100 μM BH4 and analysed by Western blotting the expression levels of p53 and Bax, one of the well-established apoptotic target genes of p53. Figure 4(A) shows that both proteins were up-regulated as early as 3 h of treatment with BH4, suggesting that p53 accumulation is associated with the acquisition of its nuclear-transacting properties. To unravel the

role of p53 in BH4-induced cell death, we knocked down p53 expression by transfecting SH-SY5Y cells with two alternative siRNAs against p53 and analysed apoptotic extent upon treatment with BH4. As shown in Figure 4(B) and Supplementary Figure S4 (at http://www.BiochemJ.org/bj/430/bj4300439add.htm), the percentage of apoptotic cells was significantly reduced in p53-silenced cells with respect to their non-targeting controls. Moreover, in line with the decreased apoptotic extent, Western blots depicted in Figure 4(C) show that p53 and Bax were only slightly up-regulated in p53-silenced cells, confirming that the p53/Bax axis contributes to BH4-induced apoptosis. To gain insight into the relevance of p53 in BH4-induced cell death, we analysed its activation in PCNs. According to the current view, following its stabilization, p53 translocates into the nucleus in order to activate the transcription of its target genes. Therefore we analysed p53 localization in PCNs upon 24 h of treatment with 1 μM BH4 by means of fluorescence microscopy. Figure 4(D) shows that BH4 challenge induced an increase in nuclear-containing p53 cells ($+36.3 \pm 2.5\,\%$) with respect to untreated neurons. We inhibited p53 activity with its specific chemical inhibitor pifithrin-α and evaluated the apoptosis extent after 24 h of treatment with 1 μM BH4. Figure 4(E) shows that pre-treatment with 20 μM pifithrin-α induced a reliable recovery of cell viability, indicating that p53 activation was implicated in the occurrence of BH4-induced apoptosis in primary neurons as well.

p38^{MAPK}-mediated phosphorylative signalling responds to BH4 neurotoxicity

Several studies suggest that two stress-activated protein kinases, JNK and p38^{MAPK}, contribute to neuronal demise in many neurodegenerative diseases, as they are sensitive to ROS production. To elucidate their involvement in BH4-induced SH-SY5Y cells death, we examined their phosphorylation/activation state by Western blot analyses. Figure 5(A) shows that both phospho-p38^{MAPK} and phospho-JNK accumulated upon BH4 treatment. In particular, phospho-p38^{MAPK} rapidly increased as early as 1 h after treatment with BH4, whereas JNK phosphorylation was evident only after 3 h. In line with this observation, the phosphorylation state of their downstream transcription factor c-Jun was up-regulated after 3 h of treatment. We next inhibited JNK- and p38^{MAPK}-mediated phosphorylative signalling. In particular, Figure 5(B) shows that pre-treatment with 10 μM of both JNK inhibitors I and II did not protect SH-SY5Y cells from BH4-induced apoptosis, suggesting that JNK phospho-activation was not functional for the apoptotic commitment. By contrast, incubations with 15 μM SB203580, the selective inhibitor of p38^{MAPK}-upstream kinases MKK3/6 (MAPK kinase 3/6), induced a significant recovery of cell viability, indicating that p38^{MAPK} activation was instead implicated in the occurrence of apoptosis. To confirm its involvement in BH4-induced neuronal demise, we then knocked down p38^{MAPK} expression by two alternative siRNAs and analysed apoptosis after 24 h treatment with BH4. Figures 5(C) and 5(D) and Supplementary Figure S5(A) (at http://www.BiochemJ.org/bj/430/bj4300439add.htm) show that sip38^{MAPK} cells were highly resistant to BH4-mediated cell death with respect to their scrambled controls. Similar results were obtained by transfecting the cells with the p38^{MAPK} dominant-negative form p38-AF (p38-AF cells), which provides a non-phosphorylatable mutant of the α1 subunit of p38^{MAPK} (Supplementary Figure S5C). To corroborate these results, we evaluated the involvement of p38^{MAPK} in apoptotic induction of PCNs as well. Western blot analyses demonstrated that phospho-p38^{MAPK} accumulated time-dependently as early as 6 h of treatment with 1 μM BH4 (Figure 5E). Moreover, its pharmacological inhibition resulted in an almost complete recovery of neuron viability after 24 h challenge with 1 μM BH4 (Figure 5F), confirming that the engagement of the p38^{MAPK}-mediated signalling pathway is fundamental for the neuronal apoptosis induced by BH4.

p38^{MAPK} activation contributes to p53 up-regulation upon BH4 treatment

p38^{MAPK} can phosphorylate p53 at multiple sites, thus promoting its stabilization and nuclear accumulation in response to various genotoxic stimuli and neurotoxins [14,37]. Therefore we investigated the occurrence of a functional connection between these two proteins under our experimental conditions. Figure 6(A) shows that the silencing of p38^{MAPK} strongly decreased p53 immunoreactive levels upon 3 and 6 h-treatment with BH4. Similar results were obtained both in sip38-2 cells (Supplementary Figure S5B) and in p38-AF cells (Supplementary Figure S5D), indicating that p38^{MAPK} up-regulated p53. To confirm the functional link between p38^{MAPK} and p53 in neurons, we pharmacologically inhibited p38^{MAPK} activation and evaluated p53 localization by fluorescence microscopy after 24 h of treatment with 1 μM BH4. Figure 6(B) shows that, in line with the recovery of neuron viability (see Figure 5F), pre-treatment with 15 μM SB203580 induced a consistent decrease in cells displaying nuclear accumulation of p53, indicating that the p38^{MAPK}/p53 signalling axis engagement is also operative during apoptosis in neuronal cells.

Oxidative stress and glucose availability modulate BH4-induced p38^{MAPK}/p53 signalling pathway activation in neuronal cells

To clarify whether oxidative stress was the upstream event underlying p38^{MAPK}/p53 activation, we pre-incubated SH-SY5Y cells for 12 h with 1 mM BSO. Figure 7(A) shows that, under these conditions, phospho-p38^{MAPK} and p53 immunoreactive bands were enhanced with respect to BH4 treatment alone, confirming that the increase in apoptotic extent, obtained upon GSH depletion (Figure 2G), was associated with the activation of the p38^{MAPK}/p53 signalling axis. Moreover, we performed treatment with BH4 in the presence of 1 μM catalase or upon 12 h of incubation with 5 mM NAC. Figure 7(B) shows that, consistent with the recovery of cell viability and ROS scavenging (see Figure 2F), catalase and NAC also reduced phospho-p38^{MAPK} and p53 levels after 3 and 6 h of treatment. The involvement of ROS in the activation of p38^{MAPK} and p53 was also found to be operative in PCNs. Indeed, catalase decreased the percentage of neurons displaying nuclear accumulation of phospho-p38^{MAPK} and p53 (Figure 7C), confirming that, upon BH4 treatment, the engagement of the p38^{MAPK}/p53 pathway is a ROS-dependent event.

To clarify the role of the inhibition of glucose uptake in the sequence of events induced by BH4, we set up growth conditions mimicking glucose deprivation. In particular, we cultured SH-SY5Y cells in 10 % of non-essential amino acids and FCS-enriched HBSS medium [7] in the presence (16 mM) or absence of glucose. We then treated the cells with 50 and 100 μM BH4 and analysed apoptosis cytofluorimetrically after 24 h of treatment. Figure 7(D) shows that the cells grown in glucose-free conditions were more sensitive to BH4 than those cultured in the presence of glucose. To correlate these effects with the activation of the p38^{MAPK}/p53 pathway, we performed further Western blot analyses. Figure 7(E) shows that phospho-p38^{MAPK} levels and p53 expression significantly increased in conditions of glucose starvation. Glucose restriction was able to modulate viability and

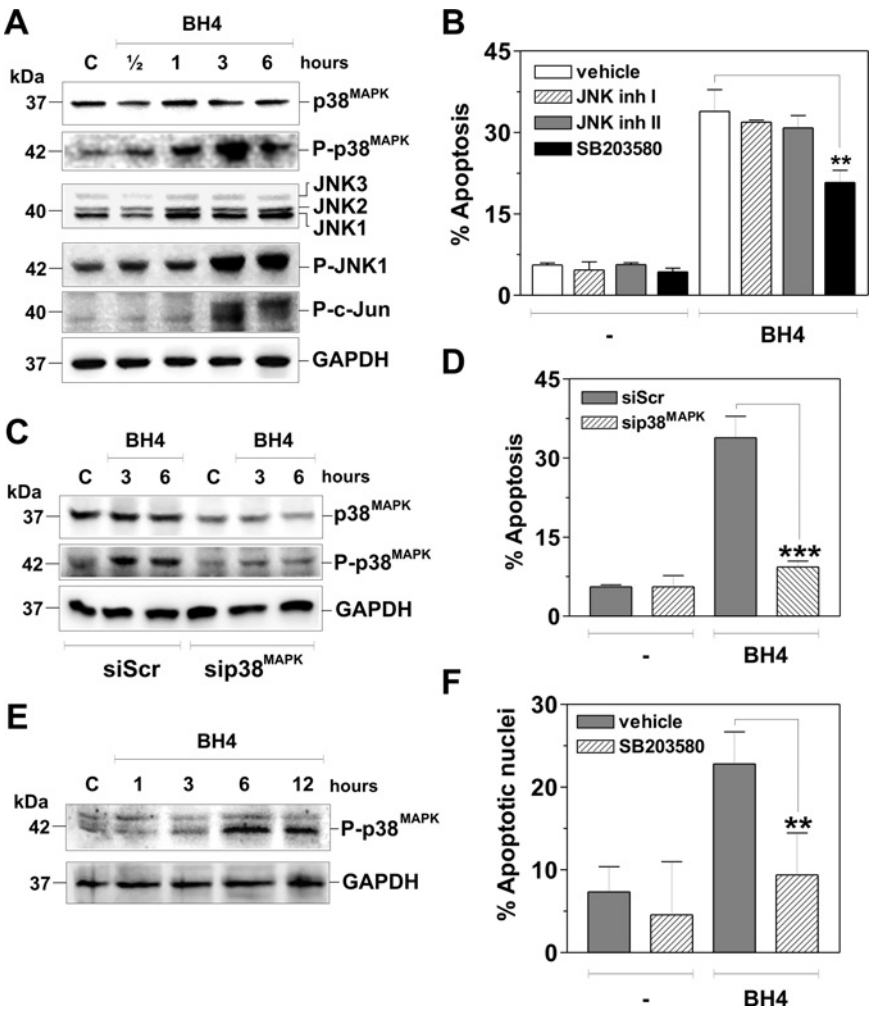

Figure 5 p38MAPK activation mediates BH4-induced apoptosis

(**A**) SH-SY5Y cells were treated with 100 μM BH4. At the indicated times, cells were lysed and 30 μg of total cell extracts were loaded for the immunodetection of basal and phospho-activated forms of p38^{MAPK} and JNK, as well as phospho-c-Jun. GAPDH was used as a loading control. Immunoblots are from one experiment representative of three that gave similar results. (**B**) SH-SY5Y cells were incubated for 1 h with 10 μM JNK inhibitors I and II, 15 μM p38^{MAPK} inhibitor SB203580, or with vehicle alone, then were treated with 100 μM BH4. After 24 h they were washed and stained with propidium iodide for the detection of apoptotic cells. Data are expressed as percentages of apoptosis and are means $\pm$ S.D., $n = 6$. $^{**}P < 0.01$. (**C**) SH-SY5Y cells were transiently transfected with SignalSilence® Pool p38^{MAPK} siRNA (sip38^{MAPK}) or with a scramble siRNA duplex (siScr). Cell adhesion was allowed for 12 h, then the cells were treated with 100 μM BH4. At the indicated times, cells were lysed and 30 μg of total cell extracts were loaded for the immunodetection of basal and phosphorylated activated forms of p38^{MAPK}. GAPDH was used as a loading control. Immunoblots are from one experiment representative of three that gave similar results. (**D**) After 12 h of adhesion, sip38^{MAPK} or siScr cells were treated with 100 μM BH4 for the next 24 h, washed and stained with propidium iodide for the detection of apoptotic cells. Data are expressed as percentages of apoptosis and are means $\pm$ S.D., $n = 6$. $^{***}P < 0.001$. (**E**) PCNs were treated with 1 μM BH4. At the indicated times, cells were lysed and 30 μg of total cell extracts were loaded for the immuno-detection of the phospho-activated forms of p38^{MAPK}. GAPDH was used as a loading control. Immunoblots are from one experiment representative of three that gave similar results. (**F**) PCNs were treated with 1 μM BH4 in the presence or absence of 15 μM SB203580. After 24 h, cells were stained with Hoechst 33342 and condensed or fragmented nuclei were counted as apoptotic. Data are expressed as percentages of apoptotic nuclei. Values are means $\pm$ S.D. ($n = 5$). $^{**}P < 0.01$.

the engagement of p38^{MAPK}/p53 signalling axis of PCNs as well. In fact, PCNs grown in glucose-deprived medium were more sensitive to BH4 treatment (Figure 7F) as well as showing a more pronounced nuclear localization of phospho-p38^{MAPK} and p53 (Figure 7G) than glucose-fed counterparts. These results provided evidence for a pivotal role of glucose in the activation of the BH4-elicited pro-apoptotic signalling pathway, but a relationship between the extent of oxidative damage and glucose availability was not shown yet. To directly examine this issue, we analysed the phospho-activation of the histone H2A.X (P-H2A.X) in glucose deprivation conditions. Figure 7(H) shows that PCNs grown in glucose-free medium displayed a larger amount of discrete P-H2A.X-positive nuclear foci with respect to glucose-fed neurons, providing a clear-cut evidence for the pivotal role of glucose in the tolerance of neuronal cells to the pro-apoptotic insult elicited after BH4 challenge.

DISCUSSION

BH4 has been suggested to participate in neuronal demise, causing cellular and biochemical alterations consistent with the current view of PD pathogenesis [16–18]; however, the molecular mechanisms responsible for its neurotoxic properties remain largely unsolved. In the present study, we demonstrated that p38^{MAPK} is responsible for the induction of the mitochondrial route of apoptosis both in SH-SY5Y neuroblastoma cells and mouse PCNs through the activation of p53. Our results clearly indicate

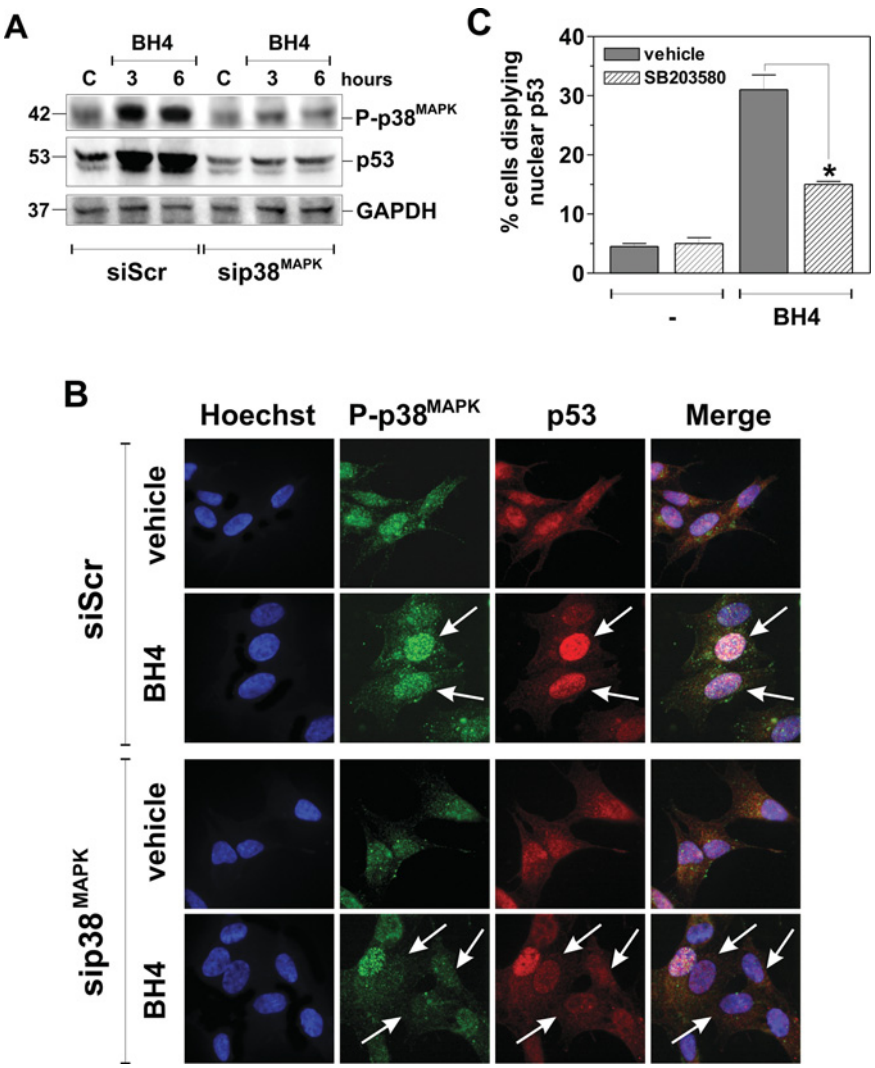

Figure 6 p38^{MAPK} regulates p53 activation

(**A**) SH-SY5Y cells were transiently transfected with SignalSilence® Pool p38^{MAPK} siRNA (sip38^{MAPK}) or with a scramble siRNA duplex (siScr). Cell adhesion was allowed for 12 h, then the cells were treated with 100 μM BH4. At the indicated times, cells were lysed and 30 μg of total cell extracts were loaded for the immunodetection of phospho-p38^{MAPK} and p53. GAPDH was used as a loading control. Immunoblots are from one experiment representative of three that gave similar results. (**B**) sip38^{MAPK} and siScr cells were treated with 100 μM BH4 for 6 h, washed, fixed in 4% paraformaldehyde and permeabilized. Phospho-p38^{MAPK} and p53 were visualized upon staining with specific antibodies, which were detected with Alexa Fluor®-488- and Alexa Fluor®-568-conjugated secondary antibodies respectively. To visualize nuclei, cells were also incubated with the cell-permeant DNA dye Hoechst 33342. Images reported are from one experiment of three that gave similar results. (**C**) PCNs were treated with 1 μM BH4 in the presence of 15 μM SB203580. After 24 h, cells were washed, fixed in 4% paraformaldehyde and subjected to immunostaining with an anti-p53 antibody and further probed with Alexa Fluor®-568-conjugated secondary antibody. Nuclei were stained with Hoechst 33342. Quantitative analyses of cells displaying nuclear p53 localization are shown. Values are means $\pm$ S.D. ($n = 5$) *$P < 0.05$.

an increased oxidative damage to proteins and DNA during BH4 exposure. In agreement with its pro-oxidant capacity, BH4 neurotoxicity is attenuated by NAC and completely counteracted by catalase administration, confirming, as previously reported in tumour cell lines [32], that H_2O_2, generated during BH4 extracellular redox cycling, is principally responsible for this toxicity. Moreover, a prominent role in cellular buffering capacity is shown for GSH, whose content decreases upon BH4 exposure as a result of BH4-induced oxidative unbalance, and whose chemical depletion enhances the sensitivity of neurons to BH4-mediated cell death. Therefore, on the basis of data from a previous study indicating GSH decrease as an important pathogenic change in the early stages of PD [38], our results from the present study suggest that BH4 acting in the micromolar range could be an intrinsic factor contributing to neuronal vulnerability, particularly in circumstances predisposing the cells to oxidative insults.

Pro-oxidant conditions occurring upon BH4 administration are responsible for the activation of p38^{MAPK}, which is the fundamental mediator of commitment to cell death, as demonstrated by a near complete restoration of cell viability obtained by silencing its expression and preventing its activation by means of two alternative siRNAs and a non-phosphorylatable dominant-negative form respectively. On the other hand, we observe a less significant attenuation of apoptosis when the cells are pre-treated with SB203580, suggesting that the canonical ROS-induced ASK1 (apoptosis signal-regulating kinase 1)-dependent phosphorylation of MKK3/6 pathway is operative, but not exclusive in mediating p38^{MAPK} activation upon

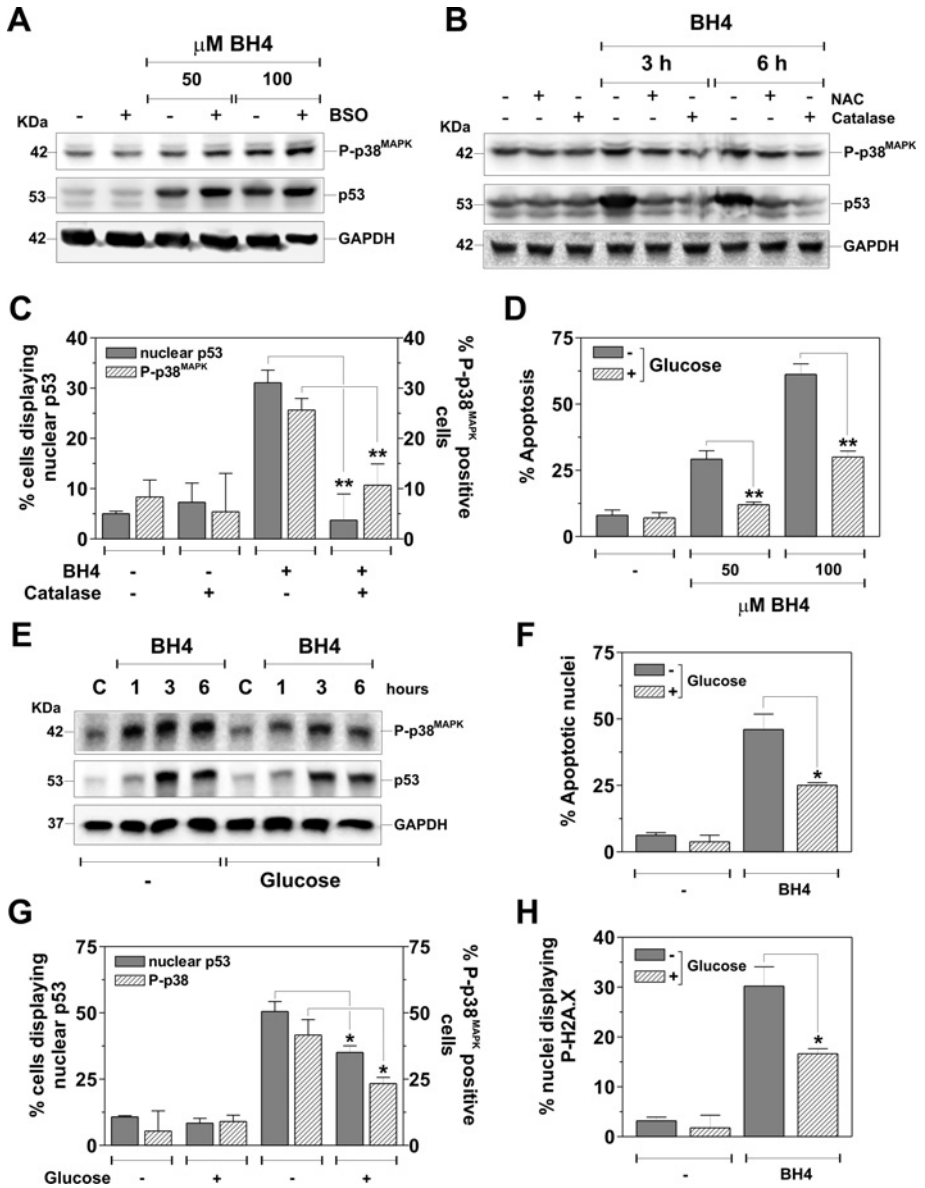

Figure 7 BH4-produced ROS and glucose availability influence p38MAPK/p53 signalling axis activation

(**A**) SH-SY5Y cells were treated with 50 or 100 μM BH4 upon 12 h of incubation with 1 mM BSO. After 6 h, cells were lysed and 30 μg of total cell extracts were loaded for the immunodetection of phospho-p38^{MAPK} and p53. GAPDH was used as a loading control. Immunoblots are from one experiment representative of three that gave similar results. (**B**) SH-SY5Y cells were treated with 100 μM BH4 upon 12 h of incubation with 5 mM NAC or in the presence of 1 μM catalase. After 3 and 6 h, cells were lysed and 30 μg of total cell extracts were loaded for the immunodetection of phospho-p38^{MAPK} and p53. GAPDH was used as a loading control. Immunoblots are from one representative experiment of three that gave similar results. (**C**) PCNs were treated with 1 μM BH4 in the presence of 15 μM SB203580. After 24 h, cells were washed, fixed in 4% paraformaldehyde and subjected to immunostaining with an anti-p53 antibody or, alternatively, with an anti-phospho-p38^{MAPK} antibody and further probed with Alexa Fluor®-568-conjugated secondary antibody. Nuclei were stained with Hoechst 33342. Quantitative analyses of cells displaying nuclear p53 localization or phosphorylated p38^{MAPK} (P-p38^{MAPK}) are shown. Values are means ± S.D. ($n = 5$). $^{**}P < 0.01$. (**D**) SH-SY5Y cells were treated with 50 or 100 μM BH4 in HBSS supplemented with 10% FCS, 0.01 mM non-essential amino acids, and 1% glutamine with or without glucose. After 24 h, cells were washed and stained with propidium iodide for the detection of apoptotic cells. Data are expressed as percentages of apoptosis and are means ± S.D., $n = 4$. $^{**}P < 0.01$. (**E**) SH-SY5Y cells were treated with 100 μM BH4 in HBSS supplemented with 10% FCS and non-essential amino acids with or without glucose. At the indicated times, cells were lysed and 30 μg of total cell extracts were loaded for the immunodetection of phospho-p38^{MAPK} and p53. GAPDH was used as a loading control. Immunoblots are from one experiment representative of three that gave similar results. Similarly, PCNs were treated with 1 μM BH4 in HBSS supplemented with B27, 0.01 mM non-essential amino acids and 1% glutamine with or without glucose. After 24 h, cells were washed, fixed in 4% paraformaldehyde and subjected to immunostaining with an anti-p53 antibody or, alternatively, with an anti phospho-p38^{MAPK} antibody and further probed with Alexa Fluor®-568-conjugated secondary antibody. Nuclear damage was evaluated by means of immunostaining with an anti-phospho-H2A.X antibody, further probed with Alexa Fluor®-488-conjugated secondary antibody. Nuclei were stained with Hoechst 33342. The percentages of cells displaying apoptotic nuclei (**F**), nuclear p53 localization and p38^{MAPK} phospho-activation (**G**), as well as discrete P-H2A.X nuclear foci (**H**) are shown. Values are means ± S.D. ($n = 5$). $^{*}P < 0.05$.

BH4 exposure. Moreover, redox unbalance, besides promoting p38^{MAPK} activation, could contribute to the stabilization of its phosphorylated form by affecting the activity of the redox-sensitive DUSP1 (dual-specificity phosphatase 1). Indeed, the catalytic cysteine of this protein phosphatase has been demonstrated to be oxidized to sulfenic acid upon oxidative conditions, leading to sustained MAPK activation [39]. Furthermore, in line with data from literature showing the ability of p38^{MAPK} to stimulate nuclear translocation of p53 in the ventral midbrain of MPTP-treated mice [14], we point

out that, in response to BH4 challenge, $p38^{MAPK}$ mediates p53 phosphorylation and its nuclear accumulation, reinforcing the functional link between these stress-responsive proteins in BH4-elicited cell demise. Since $p38^{MAPK}$ has been implicated in the post-transcriptional regulation of a number of genes containing AREs (AU-rich regions) in the 3′-UTR (3′-untranslated region) of their mRNAs [40], we could hypothesize a role for $p38^{MAPK}$ in the modulation of p53 mRNA stability, with the p53 mRNA half-life regulated by an ARE-dependent mechanism [41]. However, the only partial attenuation of p53, as a result of $p38^{MAPK}$ inhibition, suggests that other protein kinases or stimuli could directly contribute to p53 engagement.

Besides relying on the canonical pro-oxidant stimulus, we demonstrate that the $p38^{MAPK}$/p53 signalling axis is responsive to BH4-induced bioenergetic stress elicited by glucose uptake inhibition as well. Interestingly, glucose-free medium enhances $p38^{MAPK}$ phosphorylation and p53 activation, which in turn have an impact on apoptosis commitment. Ongoing investigations from our laboratory implicate AMPK as one of the energy-sensitive serine/threonine protein kinases involved in BH4-induced apoptotic commitment and in the activation of $p38^{MAPK}$/p53 signalling axis in response to reduced glucose availability.

In the sequence of events underlying BH4 toxicity, we point out that ROS production is the upstream event leading to glucose uptake inhibition, as demonstrated by the complete restoration of glucose accumulation achieved in the presence of catalase. Although the molecular mechanisms responsible for glucose uptake reduction need to be more deeply dissected, it is reasonable to hypothesize that glucose transporters could be oxidatively affected by BH4-produced ROS. Indeed, it has been reported that facilitative hexose transporters [GLUTs (glucose/hexose transporters)] display conserved cysteine residues lining the extracellular face of the pore, whose bulkier substitutions/modification could affect its size and protein function [42]. However, we cannot rule out the possibility that the GLUTs pore could be impaired by irreversible oxidative modifications involving its carbonylation or conjugation with aldehydic by-products of lipid peroxidation, as is evident from *ex vivo* models of AD [43]. Beside showing a direct effect of oxidative stress on glucose metabolism, our results from the present study also provide the evidence that the extent of BH4-induced oxidative damage and apoptosis is tightly dependent on glucose availability. Similar results were observed by Bolaños and co-workers in rat PCNs challenged with glutamate [35]. In that system, the pro-survival effect of glucose seems to rely on the enhancement of the activity of pentose phosphate pathway, which counteracts glutamate-elicited oxidative stress by generating NADPH. Similarly, our findings from the present study raise the possibility that the reduced glucose uptake observed in BH4-treated neurons could affect NADPH production, contributing to exacerbate the intrinsic pro-oxidant properties of this molecule.

Our results from the present study demonstrate that the ability to impair glucose incorporation in neurons is a feature shared with another well-defined PD neurotoxin, 6-OHDA, able to induce oxidative stress via extracellular H_2O_2 generation and $p38^{MAPK}$/p53-dependent neuronal apoptosis [14], similar to the pathway identified in the present study for BH4 neurotoxicity. Therefore we can hypothesize that the ability to affect glucose availability could be a putative common base for the induction of pro-apoptotic signalling pathways elicited by both 6-OHDA and BH4. Further investigations are ongoing in our laboratory aimed at confirming this assumption on primary dopaminergic neurons, the neuronal population mainly affected in PD.

In conclusion, the present study points out that BH4 is a particular hazard for neuronal cell integrity, because the oxidative damage derived from its redox cycles mimic the majority and most established hallmarks of PD. Our results show that ROS-dependent glucose uptake impairment contributes to BH4-induced neuronal demise through the activation of $p38^{MAPK}$/p53 signalling axis, providing a clear-cut explanation for the cytotoxicity of BH4. The present study also suggests a role for glucose uptake inhibition in the induction of pro-apoptotic pathways mediated by auto-oxidizable molecules in the pathogenesis of neurodegenerative disorders.

AUTHOR CONTRIBUTION

Simone Cardaci and Giuseppe Filomeni performed and analysed the experiments. Giuseppe Rotilio designed the research. Maria Rosa Ciriolo designed the research and wrote the paper. All authors discussed the manuscript prior to submission.

ACKNOWLEDGEMENT

We acknowledge Palma Mattioli for her technical assistance in fluorescence microscopy and image analyses.

FUNDING

This work was partially supported by grants from Ministero dell'Università e della Ricerca Scientifica (MIUR) and Ministero della Salute.

REFERENCES

1 Sofic, E., Lange, K. W., Jellinger, K. and Riederer, P. (1992) Reduced and oxidized glutathione in the substantia nigra of patients with Parkinson's disease. Neurosci. Lett. **142**, 128–130
2 Floor, E. and Wetzel, M. G. (1998) Increased protein oxidation in human substantia nigra pars compacta in comparison with basal ganglia and prefrontal cortex measured with an improved dinitrophenylhydrazine assay. J. Neurochem. **70**, 268–275
3 Huang, X., Moir, R. D., Tanzi, R. E., Bush, A. I. and Rogers, J. T. (2004) Redox-active metals, oxidative stress, and Alzheimer's disease pathology. Ann. N.Y. Acad. Sci. **1012**, 153–163
4 de Leon, M. J., Ferris, S. H., George, A. E., Christman, D. R., Fowler, J. S., Gentes, C., Reisberg, B., Gee, B., Emmerich, M., Yonekura, Y. et al. (1983) Positron emission tomographic studies of aging and Alzheimer disease. AJNR, Am. J. Neuroradiol. **4**, 568–571
5 Ma, Y. and Eidelberg, D. (2007) Functional imaging of cerebral blood flow and glucose metabolism in Parkinson's disease and Huntington's disease. Mol. Imaging Biol. **9**, 223–233
6 Arias, C., Montiel, T., Quiroz-Baez, R. and Massieu, L. (2002) β-Amyloid neurotoxicity is exacerbated during glycolysis inhibition and mitochondrial impairment in the rat hippocampus *in vivo* and in isolated nerve terminals: implications for Alzheimer's disease. Exp. Neurol. **176**, 163–174
7 Bellucci, A., Collo, G., Sarnico, I., Battistin, L., Missale, C. and Spano, P. (2008) Alpha-synuclein aggregation and cell death triggered by energy deprivation and dopamine overload are counteracted by D2/D3 receptor activation. J. Neurochem. **106**, 560–577
8 Gandhi, S., Wood-Kaczmar, A., Yao, Z., Plun-Favreau, H., Deas, E., Klupsch, K., Downward, J., Latchman, D. S., Tabrizi, S. J., Wood, N. W. et al. (2009) PINK1-associated Parkinson's disease is caused by neuronal vulnerability to calcium-induced cell death. Mol. Cell **33**, 627–638
9 Perier, C., Bové, J., Wu, D. C., Dehay, B., Choi, D. K., Jackson-Lewis, V., Rathke-Hartlieb, S., Bouillet, P., Strasser, A., Schulz, J. B. et al. (2007) Two molecular pathways initiate mitochondria-dependent dopaminergic neurodegeneration in experimental Parkinson's disease. Proc. Natl. Acad. Sci. U.S.A. **104**, 8161–8166
10 Duan, W., Zhu, X., Ladenheim, B., Yu, Q. S., Guo, Z., Oyler, J., Cutler, R. G., Cadet, J. L., Greig, N. H. and Mattson, M. P. (2002) p53 inhibitors preserve dopamine neurons and motor function in experimental parkinsonism. Ann. Neurol. **52**, 597–606
11 Trimmer, P. A., Smith, T. S., Jung, A. B. and Bennett, Jr, J. P. (1996) Dopamine neurons from transgenic mice with a knockout of the p53 gene resist MPTP neurotoxicity. Neurodegeneration **5**, 233–239
12 Gomez-Lazaro, M., Galindo, M. F., Concannon, C. G., Segura, M. F., Fernandez-Gomez, F. J., Llecha, N., Comella, J. X., Prehn, J. H. and Jordan, J. (2008) 6-Hydroxydopamine activates the mitochondrial apoptosis pathway through p38 MAPK-mediated, p53-independent activation of Bax and PUMA. J. Neurochem. **104**, 1599–1612

13 Savage, M. J., Lin, Y. G., Ciallella, J. R., Flood, D. G. and Scott, R. W. (2002) Activation of c-Jun N-terminal kinase and p38 in an Alzheimer's disease model is associated with amyloid deposition. J. Neurosci. **22**, 3376–3385

14 Karunakaran, S., Saeed, U., Mishra, M., Valli, R. K., Joshi, S. D., Meka, D. P., Seth, P. and Ravindranath, V. (2008) Selective activation of p38 mitogen-activated protein kinase in dopaminergic neurons of substantia nigra leads to nuclear translocation of p53 in 1-methyl-4-phenyl-1,2,3,6-tetrahydropyridine-treated mice. J. Neurosci. **28**, 12500–12509

15 Choi, H. J., Kim, S. W., Lee, S. Y. and Hwang, O. (2003) Dopamine-dependent cytotoxicity of tetrahydrobiopterin: a possible mechanism for selective neurodegeneration in Parkinson's disease. J. Neurochem. **86**, 143–152

16 Lee, S. Y., Moon, Y., Hee Choi, D., Jin Choi, H. and Hwang, O. (2007) Particular vulnerability of rat mesencephalic dopaminergic neurons to tetrahydrobiopterin: relevance to Parkinson's disease. Neurobiol. Dis. **25**, 112–120

17 Kim, S. W., Jang, Y. J., Chang, J. W. and Hwang, O. (2003) Degeneration of the nigrostriatal pathway and induction of motor deficit bytetrahydrobiopterin: an *in vivo* model relevant to Parkinson's disease. Neurobiol. Dis. **13**, 167–176

18 Kim, S. T., Chang, J. W., Hong, H. N. and Hwang, O. (2004) Loss of striatal dopaminergic fibers after intraventricular injection of tetrahydrobiopterin in rat brain. Neurosci. Lett. **359**, 69–72

19 Levine, R. A., Miller, L. P. and Lovenberg, W. (1981) Tetrahydrobiopterin in striatum: localization in dopamine nerve terminals and role in catecholamine synthesis. Science **214**, 919–921

20 Hwang, O., Choi, H. J. and Park, S. Y. (1999) Up-regulation of GTP cyclohydrolase I and tetrahydrobiopterin by calcium influx. NeuroReport **10**, 3611–3614

21 Kim, S. T., Chang, J. W., Choi, J. H., Kim, S. W. and Hwang, O. (2005) Immobilization stress causes increases in tetrahydrobiopterin, dopamine, and neuromelanin and oxidative damage in the nigrostriatal system. J. Neurochem. **95**, 89–98

22 Cho, S., Volpe, B. T., Bae, Y., Hwang, O., Choi, H. J., Gal, J., Park, L. C., Chu, C. K., Du, J. and Joh, T. H. (1999) Blockade of tetrahydrobiopterin synthesis protects neurons after transient forebrain ischemia in rat: a novel role for the cofactor. J. Neurosci. **19**, 878–889

23 Kirsch, M., Korth, H. G., Stenert, V., Sustmann, R. and de Groot, H. (2003) The autoxidation of tetrahydrobiopterin revisited. Proof of superoxide formation from reaction of tetrahydrobiopterin with molecular oxygen. J. Biol. Chem. **278**, 24481–24490

24 Reference deleted

25 Filomeni, G., Cerchiaro, G., Da Costa Ferreira, A. M., De Martino, A., Pedersen, J. Z., Rotilio, G. and Ciriolo, M. R. (2007) Pro-apoptotic activity of novel Isatin-Schiff base copper(II) complexes depends on oxidative stress induction and organelle-selective damage. J. Biol. Chem. **282**, 12010–12021

26 Nicoletti, I., Migliorati, G., Pagliacci, M. C., Grignani, F. and Riccardi, C. (1991) A rapid and simple method for measuring thymocyte apoptosis by propidium iodide staining and flow cytometry. J. Immunol. Methods **139**, 271–279

27 Filomeni, G., Rotilio, G. and Ciriolo, M. R. (2003) Glutathione disulfide induces apoptosis in U937 cells by a redox-mediated p38 MAP kinase pathway. FASEB J. **17**, 64–66

28 Filomeni, G., Aquilano, K., Rotilio, G. and Ciriolo, M. R. (2003) Reactive oxygen species-dependent c-Jun NH2-terminal kinase/c-Jun signaling cascade mediates neuroblastoma cell death induced by diallyl disulfide. Cancer Res. **63**, 5940–5949

29 Cardaci, S., Filomeni, G., Rotilio, G. and Ciriolo, M. R. (2008) Reactive oxygen species mediate p53 activation and apoptosis induced by sodium nitroprusside in SH-SY5Y cells. Mol. Pharmacol. **74**, 1234–1245

30 Filomeni, G., Desideri, E., Cardaci, S., Graziani, I., Piccirillo, S., Rotilio, G. and Ciriolo, M. R. (2010) Carcinoma cells activate AMP-activated protein kinase-dependent autophagy as survival response to kaempferol-mediated energetic impairment. Autophagy **6**, 202–216

31 Lowry, O. H., Rosebrough, N. J., Farr, A. L. and Randall, R. J. (1951) Protein measurement with the Folin phenol reagent. J. Biol. Chem. **193**, 265–275

32 Choi, H. J., Jang, Y. J., Kim, H. J. and Hwang, O. (2000) Tetrahydrobiopterin is released from and causes preferential death of catecholaminergic cells by oxidative stress. Mol. Pharmacol. **58**, 633–640

33 Chongthammakun, V., Sanvarinda, Y. and Chongthammakun, S. (2009) Reactive oxygen species production and MAPK activation are implicated in tetrahydrobiopterin-induced SH-SY5Y cell death. Neurosci. Lett. **449**, 178–182

34 Nakamura, K., Wang, W. and Kang, U. J. (1997) The role of glutathione in dopaminergic neuronal survival. J. Neurochem. **69**, 1850–1858

35 Delgado-Esteban, M., Almeida, A. and Bolaños, J. P. (2000) D-Glucose prevents glutathione oxidation and mitochondrial damage after glutamate receptor stimulation in rat cortical primary neurons. J. Neurochem. **75**, 1618–1624

36 Hardie, D. G. (2007) AMP-activated/SNF1 protein kinases: conserved guardians of cellular energy. Nat. Rev. Mol. Cell Biol. **8**, 774–785

37 Piccirillo, S., Filomeni, G., Brüne, B., Rotilio, G. and Ciriolo, M. R. (2009) Redox mechanisms involved in the selective activation of Nrf2-mediated resistance versus p53-dependent apoptosis in adenocarcinoma cells. J. Biol. Chem. **284**, 27721–27733

38 Sian, J., Dexter, D. T., Lees, A. J., Daniel, S., Agid, Y., Javoy-Agid, F., Jenner, P. and Marsden, C. D. (1994) Alterations in glutathione levels in Parkinson's disease and other neurodegenerative disorders affecting basal ganglia. Ann. Neurol. **36**, 348–355

39 Kamata, H., Honda, S., Maeda, S., Chang, L., Hirata, H. and Karin, M. (2005) Reactive oxygen species promote TNFα-induced death and sustained JNK activation by inhibiting MAP kinase phosphatases. Cell **120**, 649–661.

40 Frevel, M. A. E., Bakheet, T., Silva, A. M., Hissong, J. G., Khabar, K. S. A. and Williams, B. R. G. (2003) p38 mitogen-activated protein kinase-dependent and -independent signaling of mRNA stability of AU-rich element-containing transcripts. Mol. Cell. Biol. **23**, 425–436

41 Vilborg, A., Glahder, J. A., Wilhelm, M. T., Bersani, C., Corcoran, M., Mahmoudi, S., Rosenstierne, M., Grandér, D., Farnebo, M., Norrild, B. and Wiman, K. G. (2009) The p53 target Wig-1 regulates p53 mRNA stability through an AU-rich element. Proc. Natl. Acad. Sci. U.S.A. **106**, 15756–15761

42 Simpson, I. A., Dwyer, D., Malide, D., Moley, K. H., Travis, A. and Vannucci, S. J. (2008) The facilitative glucose transporter GLUT3: 20 years of distinction. Am. J. Physiol. Endocrinol. Metab. **295**, 242–253

43 Mark, R. J., Pang, Z., Geddes, J. W., Uchida, K. and Mattson, M. P. (1997) Amyloid beta-peptide impairs glucose transport in hippocampal and cortical neurons: involvement of membrane lipid peroxidation. J. Neurosci. **17**, 1046–1054

Received 6 April 2010/17 June 2010; accepted 30 June 2010
Published as BJ Immediate Publication 30 June 2010, doi:10.1042/BJ20100503

Biochem. J. (2010) **430**, 439–451 (Printed in Great Britain) doi:10.1042/BJ20100503

SUPPLEMENTARY ONLINE DATA

p38^{MAPK}/p53 signalling axis mediates neuronal apoptosis in response to tetrahydrobiopterin-induced oxidative stress and glucose uptake inhibition: implication for neurodegeneration

Simone CARDACI*[1], Giuseppe FILOMENI*[1], Giuseppe ROTILIO*† and Maria R. CIRIOLO*†[2]

*Department of Biology, University of Rome "Tor Vergata", Via della Ricerca Scientifica 1, 00133 Rome, Italy, and †Research Centre IRCCS San Raffaele - Pisana, Via dei Bonacolsi, 00163 Rome, Italy

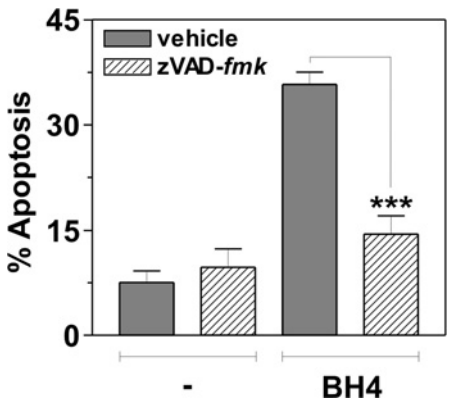

Figure S1 BH4 induces caspase-dependent apoptosis in SH-SY5Y cells

SH-SY5Y cells were incubated for 1 h with or without 20 μM of the pan-caspase inhibitor Z-VAD-FMK, treated with 100 μM BH4 for 24 h, then washed and stained with propidium iodide for the detection of apoptotic cells. Data are expressed as percentages of apoptosis and are means $\pm$ S.D., $n = 5$. $^{***}P < 0.001$.

[1] These authors contributed equally to this work.
[2] To whom correspondence should be addressed (email ciriolo@bio.uniroma2.it).

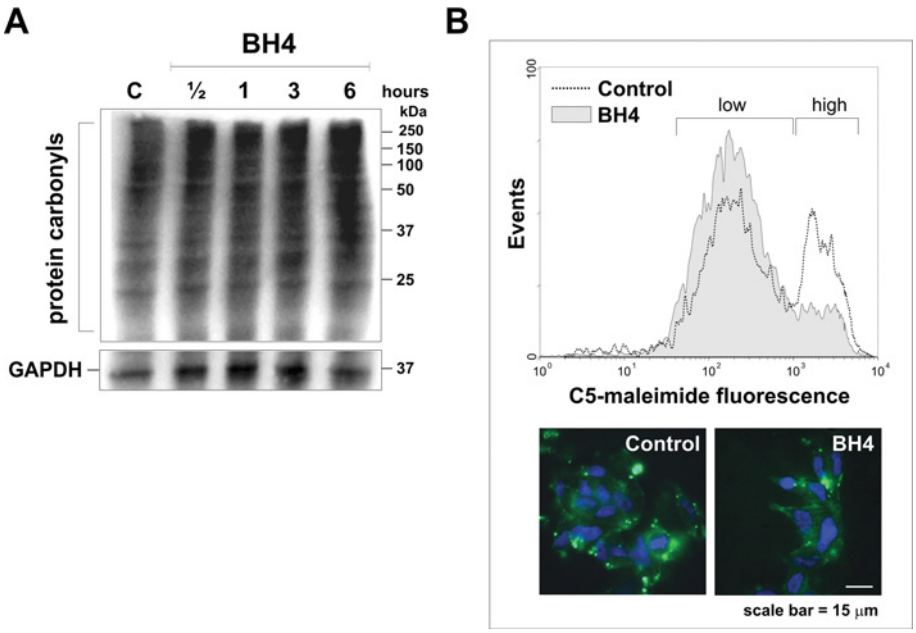

Figure S2 BH4 induces protein oxidative damage

(**A**) SH-SY5Y cells were treated with 100 μM BH4. At the indicated times, cells were lysed. Protein extracts (5 μg) were derivatized with DNP and protein carbonyls were detected by Western blot analysis using an anti-DNP antibody. The immunoblot shown is representative of four that gave similar results. (**B**) SH-SY5Y cells were treated with 100 μM BH4 for 1 h, washed and incubated with 10 μM Alexa Fluor® 488–C_5-maleimide for 15 min at 37 °C in PBS. Labelled thiols were analysed using either a FACScalibur instrument (upper panel) or fluorescence microscope (bottom panel).

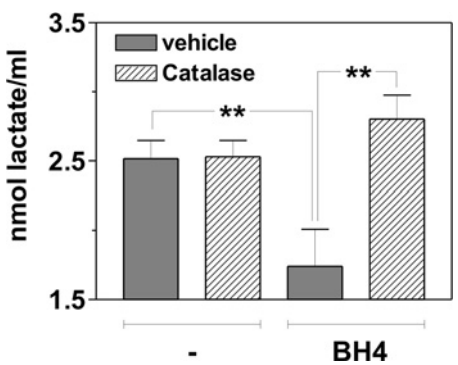

Figure S3 BH4 reduces extracellular lactate levels

SH-SY5Y cells were treated with 100 μM BH4 for 6 h in the presence or absence of 1 μM catalase. Cell media were then collected and lactate was determined spectrophotometrically following the reduction of NAD^+ at 340 nm. Data are expressed as nmol of lactate/ml and are means ± S.D. for eight independent experiments. $^{**}P < 0.01$.

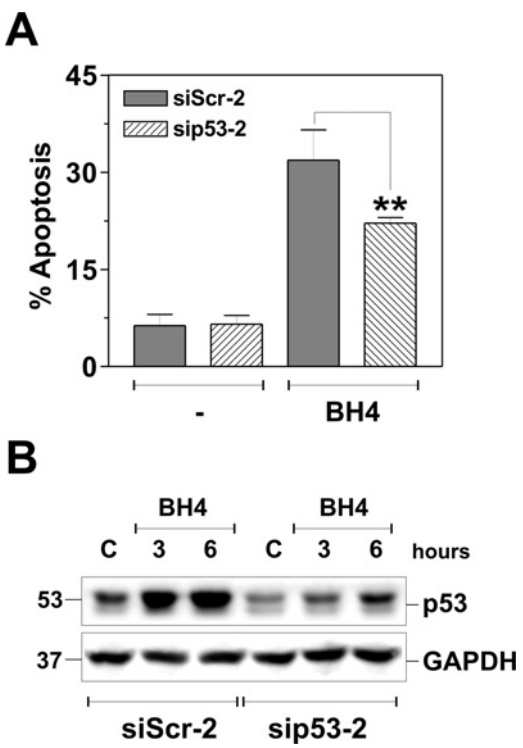

Figure S4 siRNA against p53 protects SH-SY5Y cells from BH4-induced apoptosis

(**A**) SH-SY5Y cells were transiently transfected with ON-TARGET*plus* p53 siRNA (sip53-2) or with a scramble siRNA duplex (siScr-2). Cell adhesion was allowed for 12 h, then the cells were treated with 100 μM BH4 for a further 24 h, after which they were washed and stained with propidium iodide for the detection of apoptotic cells. Data are expressed as means ± S.D., $n = 4$. $^{**}P < 0.01$. (**B**) At the indicated times, cells were lysed and 30 μg of total cell extracts were loaded for the immunodetection of p53. GAPDH was used as a loading control. The immunoblots shown are from one experiment representative of three that gave similar results.

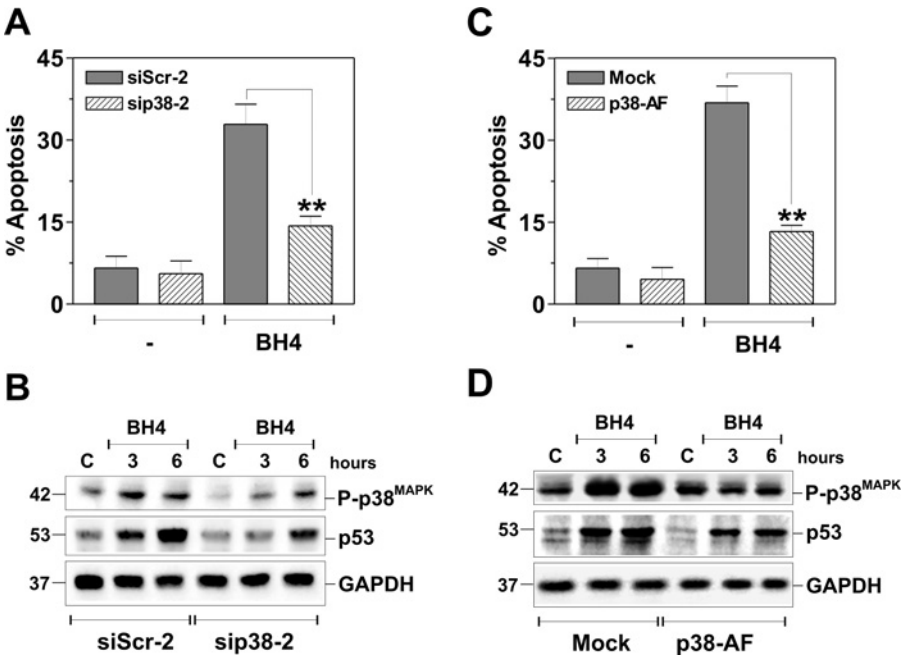

Figure S5 siRNA against p38^{MAPK} or expression of a non-phosphorylatable p38^{MAPK} mutant inhibits p53 accumulation and protects SH-SY5Y cells from BH4-induced apoptosis

(**A**) SH-SY5Y cells were transiently transfected with ON-TARGET*plus* p38MAPK siRNA (sip38-2) or with a scramble siRNA duplex (siScr-2). Cell adhesion was allowed for 12 h, then the cells were treated with 100 μM BH4 for further 24 h, washed and stained with propidium iodide for the detection of apoptotic cells. Data are expressed as means $\pm$ S.D., $n = 4$. $^{**}P < 0.01$. (**B**) At the indicated times, cells were lysed and 30 μg of total cell extracts were loaded for the immunodetection of phospho-p38^{MAPK} and p53. GAPDH was used as a loading control. Immunoblots are from one experiment are representative of three that gave similar results. (**C**) SH-SY5Y cells were transiently transfected with pcDNA3 empty vector (Mock) or with a pcDNA3 vector containing the non-phosphorylatable mutant of the α1 subunit of p38^{MAPK} (p38-AF). At 48 h of transfection, cells were treated with 100 μM BH4 for further 24 h, then washed and stained with propidium iodide for the detection of apoptotic cells. Data are expressed as means $\pm$ S.D., $n = 6$. $^{**}P < 0.01$. (**D**) At the indicated times, cells were lysed and 30 μg of total cell extracts were loaded for the immunodetection of phospho-p38^{MAPK} and p53. GAPDH was used as a loading control. Immunoblots shown are from one representative experiment of three that gave similar results.

Received 6 April 2010/17 June 2010; accepted 30 June 2010
Published as BJ Immediate Publication 30 June 2010, doi:10.1042/BJ20100503